Radiation vulnerability of standard and radiation-hardened optical glasses at MGy dose: Towards the design of tolerant optical systems

T. Allanche, C. Muller, P. Paillet, O. Duhamel, V. Goiffon, J. Rousson, J.P. Baudu, J.R. Macé, H. Desjonqueres, C. Monsanglant Louvet, et al.

Version of Record: https://www.sciencedirect.com/science/article/pii/S0022309322001399
Manuscript_22c21d33bd1396a4510582f8d2bc2516

Manuscript for review-only (Journal of Non-Crystalline Solids)

Radiation vulnerability of standard and radiation-hardened optical glasses at MGy dose: towards the design of tolerant optical systems

T. Allanche[1], C. Muller[1], P. Paillet[2], O. Duhamel[2], V. Goiffon[3], J. Rousson[4], J-P. Baudu[4], J-R. Macé[5], H. Desjonqueres[6], C. Monsanglant Louvet[6], A. Morana[1], Y. Ouerdane[1], A. Boukenter[1], and S. Girard[1,*]

[1] *Laboratoire Hubert Curien (LabHC), CNRS UMR 5516, Université de Saint-Etienne, 42000 Saint-Etienne, France, phone : (+33)477 915 812*
[2] *DAM, DIF, 91297 Arpajon, France*
[3] *ISAE Supaero, F-31055 Toulouse, France*
[4] *OPTSYS, F-42007 Saint Etienne, France*
[5] *ORANO, F-92400 Courbevoie, France*
[6] *Institut de Radioprotection et de Sûreté Nucléaire (IRSN), PSN-RES/SCA, 91192, Gif sur Yvette, France*
**sylvain.girard@univ-st-etienne.fr*

Abstract: Facing the need of cameras able to withstand high levels (MGy) of ionizing radiation and the limited set of radiation-hardened optical glasses available to manufacture the lenses of their optical systems (OS), we performed an evaluation of standard and radiation hardened glasses. One of our objectives was to understand if selecting only radiation hardened glasses is always the best choice to reduce OS radio-darkening that is the main radiation-induced macroscopic degradation. For this, we performed X-ray in situ measurements of the radiation-induced attenuation (RIA) up to 100 kGy(SiO_2) for several Ce-doped glasses from SCHOTT. Their responses are compared to their Ce-free counterparts. Due to the strong intrinsic attenuation of radiation hardened glasses caused by the Ce-codoping at shorter wavelengths, we found nearly no advantage to use radiation-hardened glasses at doses below 1 kGy(SiO_2). We also performed post-irradiation RIA measurements on 31 standard glasses irradiated up to 1 MGy (γ-rays). The outcome is that several standard glasses especially the ones with a low Abbe number and a high refractive index are sufficiently radiation tolerant in terms of RIA and can serve as promising alternative to rad-hard ones. The use of these glasses less affect the color rendering of OS and strongly reduce their costs.

1. Introduction

Since CMOS image sensors become more and more resistant to high ionizing radiation doses [1–4], applications emerge for color HD cameras in more and more severe environments, typically the one associated with MGy levels, that are usually very difficult to instrument with microelectronic components. Examples of such applications concern for example ITER [5–8] for which the development of vision systems is under progress to assist the remote handling operations such as pipe weld inspections in the most radiation exposed areas. Another application of interest concerns the nuclear waste management. In France, the CIGEO project (*Industrial Centre for Geological Disposal*) [9] and other dismantling applications will be strongly automated, implying to develop vision systems to support various operations. Together with the image sensors, the other sub-parts of the camera need to resist to the withstand radiation, eg. the optical system (OS) and the illumination system (IS). For the IS, we showed that the selected Light Emitting Diode (LED) technology is indeed quite intrinsically robust to ionizing radiations and allow designing efficient illumination sources [9]. Today, a strong limitation for the design of OS able to operate in radiation-rich environment concerns the very limited number of radiation-hardened (rad-hard) glasses. These glasses are called “rad-hard” as they have been shown to be less impacted by the Radiation Induced Attenuation (RIA) phenomena. Having access to a set of glasses with sufficiently different refractive index and optical characteristics remains mandatory to optimize the imaging performances of the camera in a wide spectral domain. Ideally, to

enhance the design, it is necessary to combine glasses spread across the Abbe Diagram. To overcome this limitation, the European Space Agency (ESA) already conducted a large experimental study [10,11] to investigate the γ-ray vulnerabilities of 23 commercial off-the-shelf (COTS) Ce-free glasses up to 5 kGy(H_2O). Their goal was to enlarge the accessible glass set to build space instrumentation. For example, in [11], the researchers exploit their results for space telecommunication applications and OS using Ce-free glasses were used on Mars [13]. Today, there remains a lack of data regarding the behaviors of bulk glasses, and particularly on COTS glasses, at doses exceeding 10 kGy and especially at the higher doses from 0.1 to 1 MGy levels. One of the reasons, in addition to the costs of radiation testing, is that researchers assumed that these glasses cannot sustain high doses due to very large RIA levels in the visible domain. So, usually for such high dose applications, researchers only select pure silica glasses for monochromatic imaging or use Ce-doped glasses in their designs when color imaging is requested–[5,8,9,14–17]. However, Ce-doped rad-hard glasses present several limitations:

- Today SCHOTT manufacturer has only five different glasses available and at least the BK7G18 is not always radiation resistant depending on the manufacturing batch [13],
- Ohara manufacturer has one Cerium doped glass in its catalog, and four in development since 2015 [19,20], no radiation data are available to our knowledge regarding those glasses,
- 45 glasses are possibly offered by CDGMGD [21], but with no data about their compositions and very limited data on their radiation responses,
- At least six from LZOS company have existed, but we only found one study that investigate their response under neutrons [6].

As a consequence, we decided for our CAMRAD project [1], to check the postulate that selecting rad-hard glasses for the optical system is always the best choice to limit the image degradation. For this, we performed online RIA measurements on both SCHOTT rad-hard glasses (*that are also poorly documented in the open literature, transmission up to 100 kGy in* [22] *and RIA up to the MGy level for 3 glasses in* [5,18]) and their standard counterparts presenting the same characteristics in terms of refractive index but no Ce-doping. Our *in situ* study (up to 1 MGy at a very high dose rate of 50 Gy/s) represents a worst-case scenario for most of the targeted environments as illustrated in Fig. 1. Facing interesting results during this first campaign, we then conducted a second γ-ray irradiation campaign on a larger set of COTS glasses to identify interesting candidates for further *in situ* characterization of their radiation vulnerabilities.

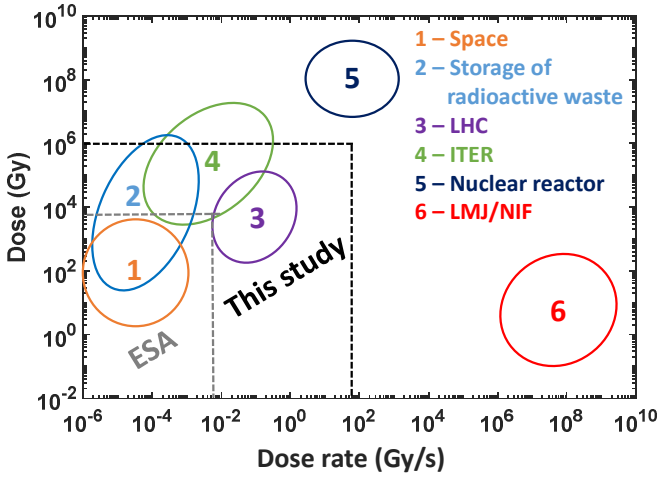

Fig. 1: Dose rate, dose and temperature associated with radiation environments of interest for optical instrumentation, as described in [23]. The ESA's area refers to [11].

2. EXPERIMENTAL PROCEDURE

2.1 In situ measurement campaign

2.1.1 Irradiation conditions and tested samples

For the online X-ray testings, we used the MOPERIX machine (100 kV X-ray tube with W-target filtered by 4 mm thick of beryllium material) that delivers X-rays beam of ~40 keV mean energy. All doses and dose rates have been measured at the sample surface exposed to the X-rays and are expressed in Gy(SiO_2) and Gy(SiO_2)/s, respectively. The temperature of the hot plate was between 33.5 and 35°C and the temperature of the sample top was between 31 and 33.7°C. T probing light beam was ~0.5 mm below the top of the glass sample. To not affect X-rays penetration, the temperature was measured on the top of a second reference sample as shown in Fig. 2.b. The glass reference and irradiation conditions are summarized in Table 1. We are focusing here on the most relevant data to compare the rad-hard glasses to standard ones, but more results are given in [9]. Each rad-hard glass is compared to its standard counterpart irradiated under the same conditions.

Table 1: Tested bulk glasses and irradiations conditions

Radiation hardened Glasses	**BK7G18**	**K5G20**	**LAK9G15**	**LF5G19**	**SF6G12**
Standard Glasses	**N-BK7**	**K5**	**N-LAK9**	**LF5**	**N-SF6**
Run#1	2.5 Gy/s up to 0.1 MGy	1.2Gy/s up to 0.1 MGy	1.2Gy/s up to 0.1 MGy	1.2Gy/s up to 0.1 MGy	1.2Gy/s up to 0.1 MGy
Run#2	2.5 Gy/s up to 0.1 MGy	2.5 Gy/s up to 0.1 MGy	2.5 Gy/s up to 0.1 MGy	2.5 Gy/s up to 0.1 MGy	2.5 Gy/s up to 0.1 MGy
Run#3	50 Gy/s up to 1 MGy	50 Gy/s up to 1 MGy	50 Gy/s up to 1 MGy	50 Gy/s up to 1 MGy	50 Gy/s up to 1 MGy

2.1.2 Online RIA measurement principle

To monitor in real-time the RIA growth during irradiation and its decay after irradiation in the whole visible domain, we used the setup detailed and validated in [18]. Compared to more usual post-irradiation measurements, *in situ* RIA allows observing the contribution of both metastable and stable defects, giving a better overview of the glass vulnerability. The setup scheme is illustrated in Fig. 2. The light from a white light source (*DH2000BAL* from Ocean Optics) is injected in a radiation hardened multimode optical fiber that is connected to a parabolic mirror (UV-Enhanced Aluminum Reflective Collimators *Thorlabs RC02SMA-F01*) allowing to obtain a parallel light beam. This beam propagates in air up to the sample under test, close to its surface. After propagation through the sample and in air, the transmitted light is then collected by a second collimator allowing the signal transport through a second optical fiber to a spectrophotometer . By monitoring the system transmission spectra before, during and after the irradiation, it is possible to calculate the RIA spectra through the formula:

$$RIA\left(\frac{dB}{mm}\right) = -\frac{10}{L} \times log_{10}\left(\frac{I_{irrad} - noise}{I_0 - noise}\right) \quad (1)$$

With L the sample length in mm, I_0 the intensity before the irradiation in count, I_{irrad} the intensity during the irradiation or the recovery in count, $noise$ the spectrometer dark signal in count.

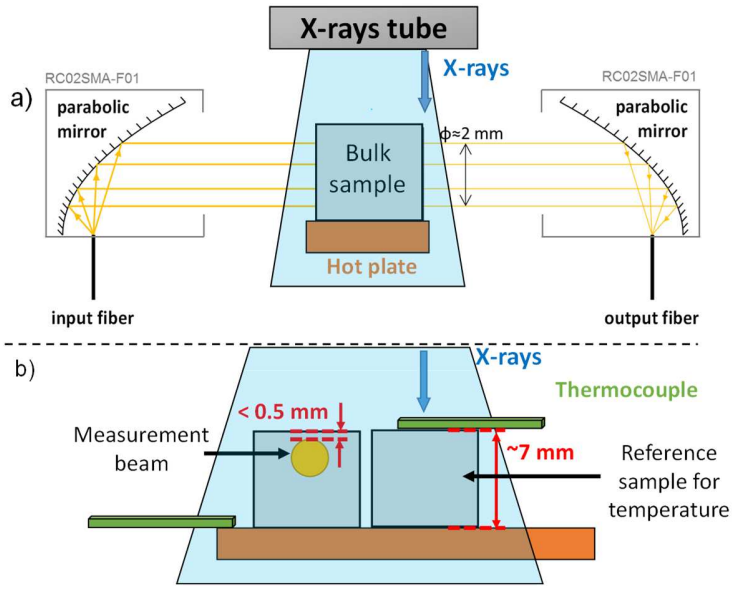

Fig. 2 : Schematic representation of the irradiation set-up, a) front view, b) side view.

2.1.3 Post-irradiation RIA measurement

For the post-irradiation absorption measurements on the bulk glasses, we used a *Carry 5000* spectrophotometer from Agilent. Its schematic diagram is reported in Fig. 3.

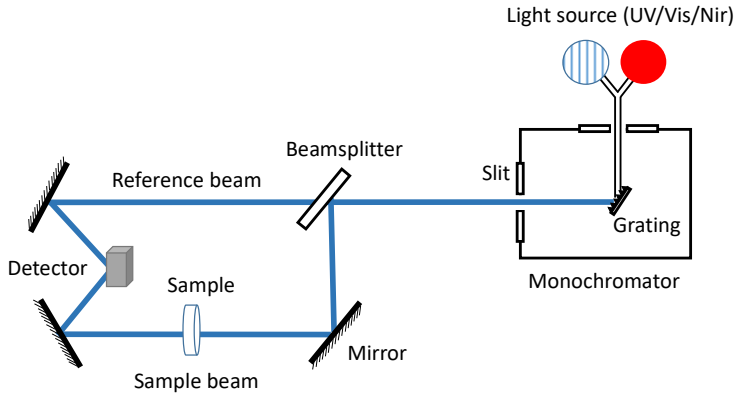

Fig. 3 : Schematic diagram of the used spectrophotometer (Carry 5000 spectrophotometer from Agilent)

The instrument uses a halogen lamp for studies in the visible spectral domain and a deuterium lamp for UV investigations. After the adjustment of the instrument's parameters (gain, acquisition time, spectral resolution...), we set a baseline. The sample is then, inserted, at normal incidence to the probe beam and many scans are repeated (and integrated) to reduce noise/signal ratio. With this instrument, RIA is computed as:

$$RIA\ (dB/mm) = \frac{A_{irradiated}}{L_{irradiated}} - \frac{A_{Pristine}}{L_{pristine}} \qquad (2)$$

With $A_{irradiated}$ the measured attenuation of the irradiated glass, $A_{Pristine}$ the attenuation of the pristine glass, $L_{irradiated}$ the length of the irradiated sample in mm and $L_{pristine}$ the length of the pristine sample in mm.

2.2 γ-ray irradiation campaign

2.2.1 Irradiation conditions

Glasses were irradiated with γ-rays in the IRMA irradiation facility at the IRSN (Saclay, France) [15] with a ^{60}Co source at doses of 0.1, 0.5 and 1 MGy respectively at 0.84, 0.42 and 0.084 Gy/s. All experiments were done at room temperature.

2.2.2 Tested samples

Facing the great complexity of those bulk glass compositions and the impossibility to predict which one could present a good response to high radiation dose [24], we used a systematic approach. We prepared at least 4 different samples of 31 different optical glasses chosen among all glass types (FK, PK,…) in order to cover as much as possible the Abbe diagram in terms of both refractive index and Abbe number. Fig. 4 illustrates the position of the selected standard and rad-hard glasses on the Abbe diagram. The SF6G05 (star in the right top corner) is the only rad-hard glasses with a high refractive index and a low abbe number, having such glass is almost mandatory to create an achromatic doublet [25] in order to compensate chromatic aberrations. Table 2 reviews for each of these glasses, its reference name, its Abbe number (v_d), its refractive index at 587.6 nm (n_d), as well as the number of recovery days before the RIA measurement with the spectrophotometer.

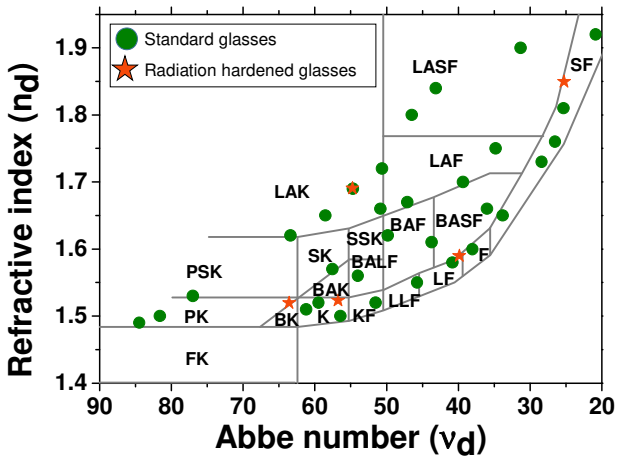

Fig. 4: Tested glasses in the Abbe diagram, green circles are standard glasses and orange stars are the 4 Schott tested rad-hard glasses (Bk7G18, K5G20, LaK9G15, LF5G19 and SF6G05)

Table 2: Name, Abbe number refractive index @ 587.6 nm and number of days between irradiation ends and the measurement day of tested glasses

Glass name	ν_d	n_d	Number of recovery days	Glass name	ν_d	n_d	Number of recovery days
F5	38.03	1.60	43	**N-LAK10**	50.62	1.72	61
K10	56.41	1.50	45	**N-LASF41**	43.13	1.84	63
LF5	40.85	1.58	44	**N-LASF44**	46.5	1.80	76
LLF1	45.75	1.55	77	**N-LASF46B**	31.32	1.90	76
N-BAF10	47.11	1.67	42	**N-PK51A**	76.98	1.53	83
N-BAF4	43.72	1.61	42	**N-PK52A**	81.61	1.50	83
N-BAK1	57.55	1.57	38	**N-PSK53A**	63.39	1.62	78
N-BASF2	36	1.66	87	**N-SF14**	26.53	1.76	83
N-BASF64	39.38	1.70	42	**N-SF2**	33.82	1.65	82
N-FK51A	84.47	1.49	44	**N-SF6**	25.36	1.81	52
N-K5	59.48	1.52	44	**N-SF66**	20.88	1.92	83
N-KF9	51.54	1.52	45	**N-SSK5**	50.88	1.66	84
N-KZF52	54.01	1.56	42	**N-SSK8**	49.83	1.62	85
N-LAF7	34.82	1.75	62	**N-ZK7**	61.19	1.51	108
N-LAK7	58.52	1.65	63	**SF10**	28.41	1.73	80
N-LAK9	54.71	1.69	73				

2.3 Sample Characterizations

The post-mortem measurements were performed between 43 and 108 days after the irradiation. The transmission spectrum of each pristine or irradiated sample was measured at least 4 times to reduce the signal to noise ratio and to estimate the error bars. To compute the RIA we compared the attenuation spectra of the pristine sample to the one of samples irradiated at various dose levels.

This experiment gives only access to the contribution from the room-temperature stable defect and then on the RIA permanently induced by the γ-rays. As we wait a minimum of 43 days before the first measurement, we could consider that the room-temperature metastable defects have been bleached and that this part of the RIA information is recovered. As shown in [11,26] and theoretically explained in [27], most of the recovery takes place during the first hours or days after the irradiation ends, after that the RIA values tend to a limit, explained by the permanent damages. As a consequence, it is possible to compare the behaviors of samples measured at different times after this situation is attained. During their storage time (see Table 2), the samples were stored at 20°C in the dark. Of course, this study allows performing a first screening of the various glasses, identifying those with low permanent RIA level that are the most interesting for a future series of online measurements.

3. RESULTS & DISCUSSION

3.1 Online results

With the X-ray online measurements, we are able to continuously record the time and spectral evolution of the RIA. In Fig. 5 we present the difference between the total losses (Fresnel reflections + internal transmission + RIA) of standard glasses (Cerium-free) and the total losses of corresponding rad-hard glasses during irradiation at different doses. If the resulting curve is under zero, that means that the standard glass has a lower attenuation at the given dose than its rad-hard counterpart, positive value is for the opposite trend (so the cerium-doping avoid RIA losses). For all glasses, at the studied dose rates there is almost no difference between both categories of glasses before 1 kGy (100 krad). Up to 10 kGy, four of the standard glasses remains more transparent in the blue part of the spectrum than their Ce-doped counterparts thanks to their lower intrinsic absorbance. Indeed, it is well-known that the Cerium-doping of silica increases the absorption in this range of wavelengths [18,28].

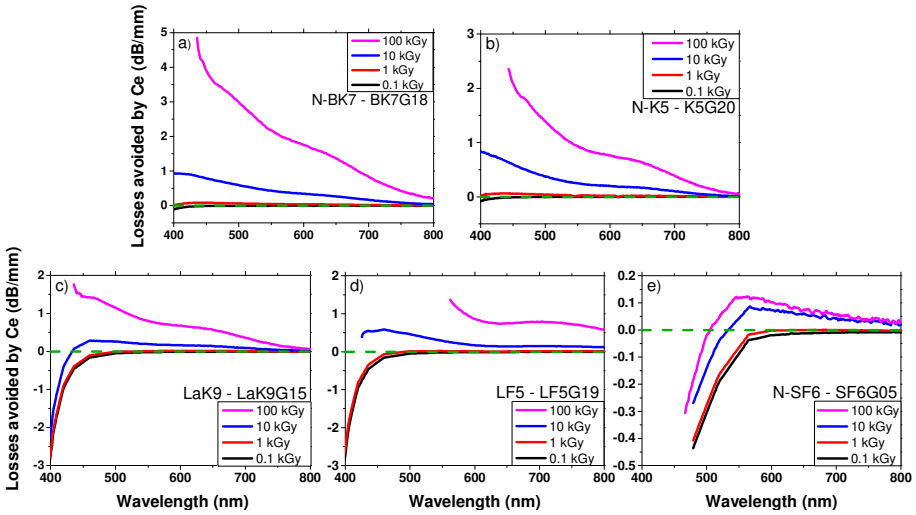

Fig. 5: Difference between the steady state X-ray RIA spectra of the standard glasses (without Ce) and hardened ones measured during irradiation at different doses and at ~30°C. a) N-BK7 – BK7G18 at 10 Gy/s) , b) N-K5 - K5G20 at 1.2 Gy/s, c) LaK9 – LaK9G15 at 1.2 Gy/s, d) LF5 – LF5G19 at 1.2 Gy/s, e) N-SF6 –-SF6G05 at 1.2 Gy/s

As it could be expected, the more the ionizing dose increases, the more the rad-hard glasses demonstrate their potential in limiting the visible RIA. For most of the glasses, Ce-doping avoids several dB/mm of RIA in this domain. There is a noticeable exception: the N-SF6/SF6G05 set of glasses. For this very important reference (as it is one of the sole flint glasses available for the OS design), we observe that at 100 kGy both glasses present very comparable RIA levels between 500 to 800 nm. If the Ce-doping of the rad-hard glass allows reducing the RIA by

about 0.1 dB/mm at 100 kGy, the standard glass has clear better performances below 500 nm. Figure 5 focuses on the N-SF6 glass, discussing its RIA spectra at different doses during irradiation (Fig.5a) and the dose rate dependence of these losses at 100 kGy. The RIA of N-SF6 saturates in the whole spectral domain after 100 kGy at 50 Gy/s and at 20 kGy at 1.2 Gy/s (Fig. 7.a and b Fig. 6.b). Its RIA level strongly decreases when lowering the dose rate (we observe the same behavior with the other standard glasses, see [9]), so we can expect that the RIA level of this standard glass will remain acceptable for most of the targeted radiation environments and architectures of optical systems and we could expect that lower the dose rate is, lower the saturation level will be.

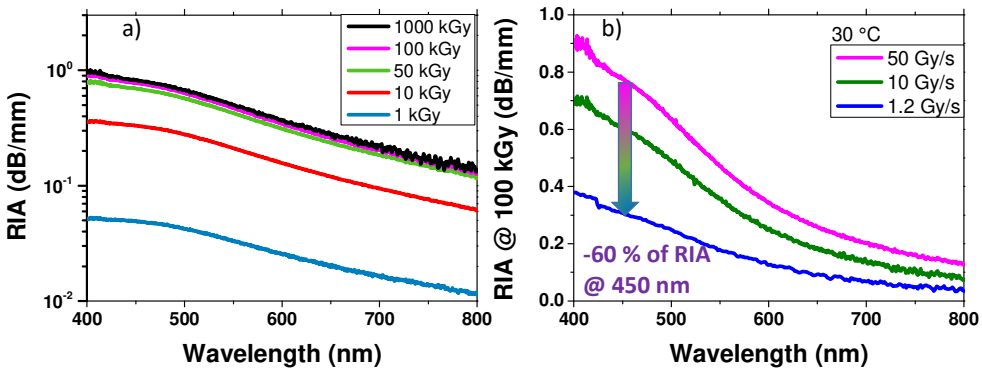

Fig. 6: N-SF6 a) RIA spectra up to 1000 kGy (50 Gy/s at 30°C), b) RIA spectral dependence at different dose rates (100 kGy at 30°C)

Fig. 7 a) presents the growth kinetics of the internal attenuation (Intrinsic + RIA) of the N-SF6 and the SF6G05 glasses. Fig.6 b) compares the spectral dependence of this attenuation at different doses. On the same figure are reported the usual color LED emissions in the blue, green and red domains. At the dose of 100 kGy (1.2 Gy/s), the N-SF6 glass exhibits a stronger RIA at 450 nm (0.6 dB/mm) than the SF6G05 (0.29 dB/mm). However, as this glass also has a lower intrinsic attenuation, it clearly offers better transmission performances for wavelengths below 460 nm. Indeed, the use of the SF6G05 induces the whole signal loss in the blue domain. As its global attenuation remains below 0.3 dB/mm over the whole spectral range of interest for the LEDs, it could be more interesting than its rad-hard counterpart for color imaging at high dose levels.

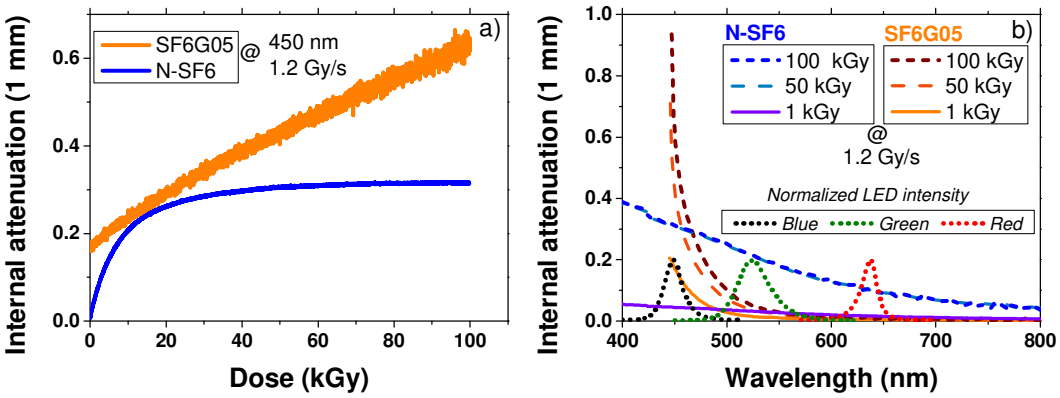

Fig. 7: SF6G05 and N-SF6 a) Comparison between the online growth kinetics of the internal attenuation (intrinsic + RIA) @ 450 nm and 1.2 Gy/s for 1 mm, b) Comparison between the spectral dependences of the internal attenuation at different doses (1.2 Gy/s) for 1 mm of the two glasses. In the figure are illustrated the typical emission spectra of blue, green and red LEDs used to design illumination systems.

Thanks to its moderate global attenuation all over the visible spectrum, a light source seen through N-SF6 will present only a small additional degradation in the red and the green channels compared to the SF6G05 case but a huge improvement of the performances in the blue domain. To highlight this, we simulated the effect of 5 mm of the two glasses on the color rendering, results are given in Fig. 8.a). It reveals that, in addition to its higher RIA in the blue part of the spectrum, the second disadvantage of the SF6G05 glass is that it affects more the natural colors, an effect that could be particularly impacting for color-dependent measurements or monitoring. Using N-SF6 as a substitute for SF6G05 results in a reasonable attenuation increase in the 500 nm to 800 nm range but a strong decrease below 500 nm. This is further demonstrated by simulating a white LED spectrum after passing through 1 mm of both glasses (Fig. 8b). The lower the dose rate, the more in favor of the N-SF6 the trade is, independently of the dose level. From our data published in [9], we deduce that the upper limit could be between 1 and 10 Gy/s, for applications as [14] associated with a dose rate lower than this threshold, the use of N-SF6 seems preferable.

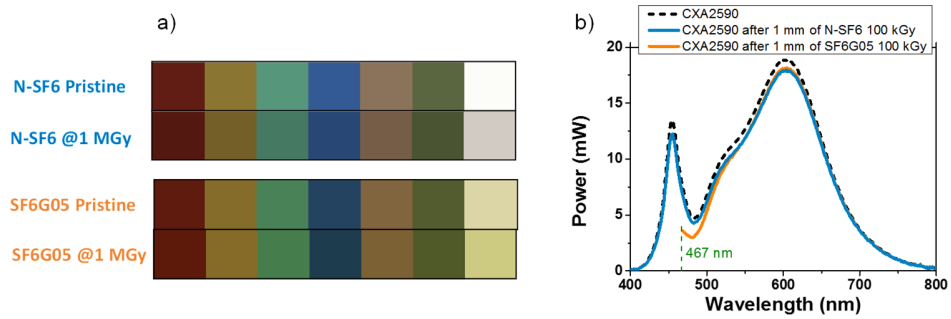

Fig. 8 : c) Comparison between the effect on color rendering of 5 mm of SF6G05 and N-SF6 glasses after 100 kGy, d) Comparison of the CXA2590 LED spectra through 1 mm of each glass irradiated at 100 kGy (under 467 nm we were not able to record the RIA level of the SF6G05 @ 100 kGy). For a, b, c & d the irradiation conditions are 1.2 Gy/s & 30°C.

3.2 Post-irradiation results

To identify the most interesting glasses, we defined a criterion based on their average permanent (post-irradiation) RIA level in the 425 to 500 nm range of wavelengths, that corresponds to the blue LED emission (Fig. 7.b). Such criteria seems pertinent as LEDs will probably be more and more used for lighting applications in radiation-rich environments [9,29,30]. For the whole set of tested glasses, the RIA decreases at larger wavelengths, so this criterion informs on the maximum RIA encountered in the visible domain. Fig. 9 reviews the Abbe diagram highlighting the RIA of the different γ-ray irradiated glasses at 0.1 and 1 MGy. These data are also listed in Table 3 for these two doses and an additional one. Fig. 10 and Table 3 also gives RIA of rad-hard glasses measured online at 0.1 MGy (1.2 Gy/s, 30°C) and 1 MGy (50 Gy/s, 30°C).

After measuring all these glasses after their γ -ray irradiation, we found that most of those located in the top right area of the Abbe diagram are naturally quite radiation resistant (*in term of permanent RIA*) and have a low permanent attenuation in the blue domain such as the N-SF14 (Fig. 9.c). This is particularly significant for optical system designers because this part of the diagram contains the glasses allowing an efficient compensation of the chromatic aberrations when combined with pure silica rad-hard glasses[5,8,18,31]. The permanent RIA of these glasses tends to saturate at higher dose (see Fig. 9.b,e,f,g,h). We choose to present the detailed results only for some relevant glasses:

- Those with high refractive index and low Abbe number, Fig. 9.a) to c)
- One glass with high refractive index and medium Abbe number because there is no equivalent rad-hard glass, Fig. 9.e

- Glasses that may replace radiation rad-hard Fig. 9.f and g.

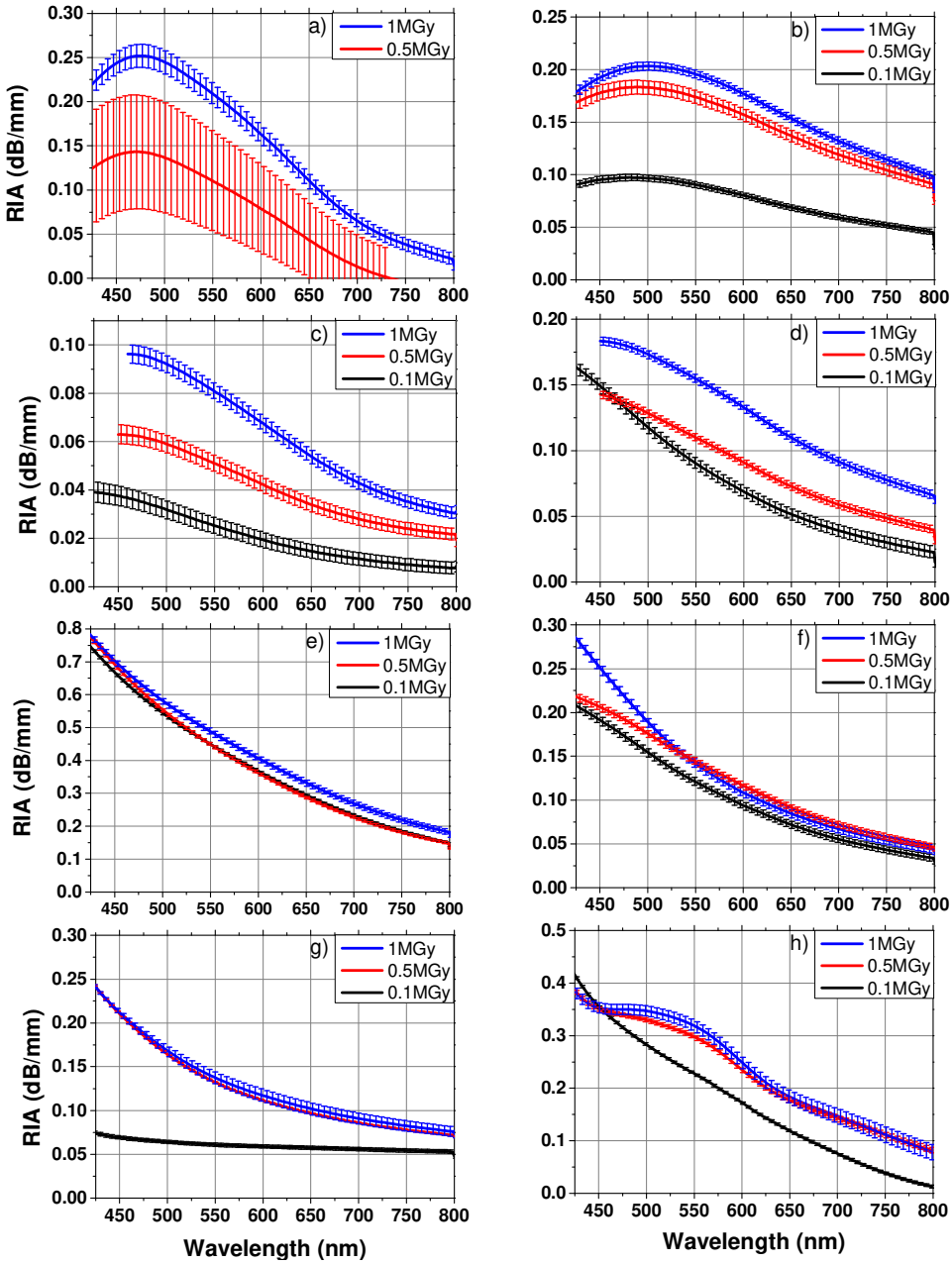

Fig. 9: RIA spectral dependence of a) N-SF66, b) N-LASF46B, c) SF14, d) N-LASF7, e) N-LASF41, f) N-SF2, g) N-BAF4, h) N-KF9, these curves represent the permanent RIA at RT.

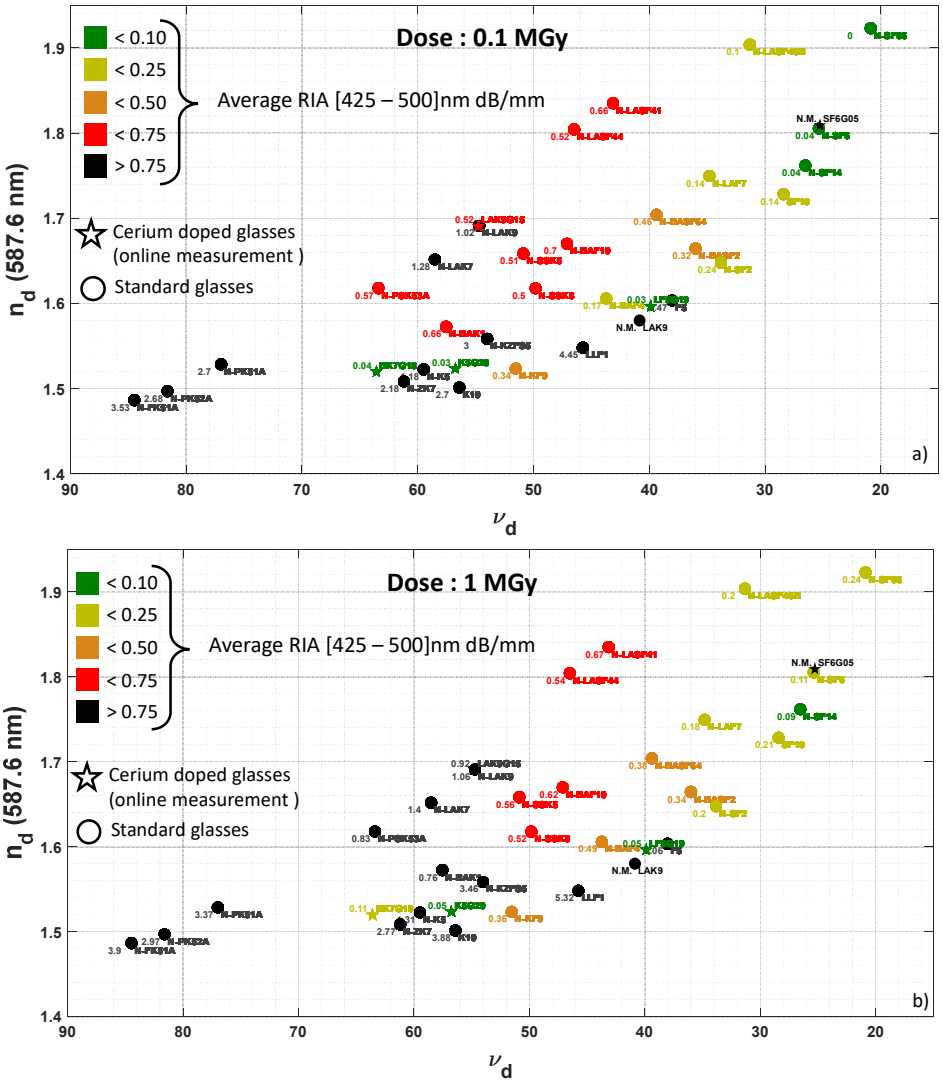

Fig. 10: Average permanent RIA of some SCHOTT standard glasses after γ-ray irradiation at a) 0.1 MGy and b) 1 MGy dose. For radiation rad-hard, at 0.1 MGy we used RIA from online measurement performed at the lower dose rate available (see Table 1), at 1 MGy we used RIA measured during irradiations performed at 50 Gy/s. *If the RIA is not measurable in the whole range between 425 and 500 nm, the RIA value is replaced by N.M.*

Table 3 : Average RIA measured between 425 and 500 nm at the 3 doses after the recovery time given in Table 2.

Glass name	RIA at 0.1 MGy	RIA at 0.5 MGy	RIA at 1 MGy	Glass name	RIA at 0.1 MGy	RIA at 0.5 MGy	RIA at 1 MGy
BK7G18	0.04	0.09	0.11	**N-LAK9**	1.02	1.05	1.06
F5	3.45	4.51	5.06	**LAK9G15**	0.52	0.87	0.92
K10	2.7	3.47	3.88	**N-LASF41**	0.66	0.64	0.67
LF5	N.M	N.M	N.M	**N-LASF44**	0.52	0.49	0.54
LF5G19	0.03	0.05	0.05	**N-LASF46B**	0.1	0.18	0.2
LLF1	4.45	5.03	5.32	**N-PK51A**	2.72	3.07	3.37
N-BAF10	0.7	0.64	0.62	**N-PK52A**	2.68	0.69	2.97
N-BAF4	0.17	0.48	0.49	**N-PSK53A**	0.57	0.86	0.83
N-BAK1	0.66	0.71	0.76	**N-SF2**	0.24	0.18	0.2
N-BASF2	0.32	0.32	0.34	**N-SF6**	0.04	0.06	0.99
N-BASF64	0.46	0.47	0.38	**SF6G05**	N.M	N.M	N.M
N-FK51A	3.53	3.77	3.9	**N-S14**	0.04	0.08	0.11
N-K5	1.18	1.25	1.31	**N-SF66**	0	0.14	0.24
K5G20	0.02	0.05	0.07	**N-SSK5**	0.51	0.55	0.56
N-KF9	0.34	0.35	0.36	**N-SSK8**	0.5	0.52	0.52
N-KZFS5	3	3.29	3.46	**N-ZK7**	2.18	2.61	2.77
N-LAF7	0.14	0.14	0.18	**SF10**	0.14	0.18	0.21
N-LAK7	1.28	1.35	1.4				

If the RIA is not measurable in the whole range between 425 and 500 nm, the RIA value is replaced by N.M.

For some glasses, the RIA is not monotonously growing with the dose as in the case of the N-BAF10 glass. This can be explained by two main hypotheses: first a difference between samples polishing, there are "homemade" and even if samples of the same glass were polished together we cannot exclude a difference in the surface quality. Second, samples can deflect the spectrometer beam depending on their shapes, it is especially visible when gratings or sources are changing. This deflection creates a jump in the absorption spectrum that can be positive or negative even for the same sample. And because for the RIA computation we are comparing irradiated samples against a pristine one, these two parameters can decrease or increase the RIA. The worst case here is the N-BASF64 with a RIA of respectively 0.47 dB/mm at 0.5 MGy and 0.38 dB/mm at 1 MGy. So we can attribute to our measurements a maximum error of ±0.09 dB/mm. This error is not changing the order of magnitude of RIA.

We do not have yet enough information on the composition of these different glasses and then cannot easily propose any hypothesis explaining the good radiation resistance of some of them. But because this will allow an easier conception of rad-hard optical systems at a lower cost [27], a future test campaign will be performed to characterize the online response of the glasses under X-ray irradiation and verify that their potential for operation under harsh environments is not affected by transient metastable defects, that could quickly recover just after the irradiation.

4. Conclusion

Studies [5,7,8,33], camera manufacturers [34–36] and glass manufacturers [19,37] that are interested in the use of glasses in radiation-rich environments (more than some kGy) do not take into account the possibility to use standard optical glasses instead of rad-hard ones. That probably comes from the long series of studies that presented the browning of non-Cerium doped glasses under radiation [10,24,26,38–41]. In our case we decided to compare rad-

hard glasses to their standard counterparts. So, we measured in situ, under X-rays, the RIA of several Schott rad-hard glasses and of their standard counterparts. We found that, at lower dose rates (1.2 Gy/s and below), Cerium-doping is not so interesting for operation in the visible domain for doses below 1 kGy (100 krad). At higher doses, Ce-doping avoids loss increase at least for wavelengths above 500 nm. However, the Ce induces high losses in the blue domain (<500 nm) and almost prevents imaging applications in this spectral range. As a consequence, the radiation response of the N-SF6, the SF6G05 counterpart, is particularly interesting. Its RIA saturates at all wavelengths (after 50 kGy at 50 Gy/s or 20 kGy at 1.2 Gy/s) at higher doses and decreases with the dose rate. If we consider the whole attenuation of the glass and not only the RIA, this glass allows reducing the impact of the Ce-doping on the color rendering and could allow designing color-camera with better performances in the visible domain.

In addition to these *in situ* tests, we carried a systematic measurement campaign on standard glasses with γ-rays. In this case, the permanent RIA spectra of the glass are measured post-irradiation after exposure at different dose levels. By this approach, we identified at least 9 glasses that are naturally quite radiation-resistant at high dose, i-e. presenting low permanent RIA levels in the visible domain. These glasses could greatly simplify the design of color imaging optical systems for harsh environments, but it should be verified that their online radiation response is not too much affected by metastable point defects.

5. References

[1] V. Goiffon, T. Allanche, C. Muller, P. Paillet, J.-R. Macé, M. Osmond, P. Burnichon, S. Plumeri, J.-P. Baudu, A. Boukenter, P. Magnan, S. Rizzolo, F. Corbière, O. Duhamel, H. Desjonqueres, R. Molina, Y. Ouerdane, T. Lépine, R. Clerc, S. Girard, CAMRAD: Development of a Multi-Megagray Radiation Hard CMOS Camera for Dismantling Operations, (2018) 10.

[2] S. Rizzolo, V. Goiffon, F. Corbiere, R. Molina, A. Chabane, S. Girard, P. Paillet, P. Magnan, A. Boukenter, T. Allanche, C. Muller, C. Monsanglant-Louvet, M. Osmond, H. Desjonqueres, J.-R. Mace, P. Burnichon, J.-P. Baudu, S. Plumeri, Radiation Hardness Comparison of CMOS Image Sensor Technologies at High Total Ionizing Dose Levels, IEEE Transactions on Nuclear Science. 66 (2019) 111–119. https://doi.org/10.1109/TNS.2018.2884037.

[3] C. Muller, T. Allanche, P. Paillet, O. Duhamel, V. Goiffon, S. Rizzolo, T. Lépine, J. Rousson, J.-P. Baudu, J.-R. Macé, H. Desjonqueres, C. Monsanglant Louvet, Y. Ouerdane, A. Boukenter, S. Girard, Investigations of the MGy dose level radiation effects on the photometric budget of a radiation-hardened CMOS-based camera, Appl. Opt. 58 (2019) 6165. https://doi.org/10.1364/AO.58.006165.

[4] S. Rizzolo, V. Goiffon, F. Corbiere, R. Molina, S. Rolando, S. Girard, P. Paillet, P. Magnan, A. Boukenter, T. Allanche, Partially Pinned Photodiode Performances for Emerging Space and Nuclear Applications, IISW2019_Proceeding. (2019).

[5] T. Allanche, P. Paillet, V. Goiffon, C. Muller, M. Van Uffelen, L. Mont-Casellas, O. Duhamel, C. Marcandella, S. Rizzolo, P. Magnan, R. Clerc, T. Lepine, M. Hebert, A. Boukenter, Y. Ouerdane, R. Scott, W. De Cock, S. Girard, Vulnerability and Hardening Studies of Optical and Illumination Systems at MGy Dose Levels, IEEE Transactions on Nuclear Science. 65 (2018) 132–140. https://doi.org/10.1109/TNS.2017.2783187.

[6] I.I. Orlovskiy, K.Yu. Vukolov, E.N. Andreenko, M.N. Gulyukin, Neutron irradiation of flint glasses for optics in ITER, Nuclear Materials and Energy. 15 (2018) 249–253. https://doi.org/10.1016/j.nme.2018.05.009.

[7] A. Moroño, R. Vila, E.R. Hodgson, KU1 and KS-4V quartz glass lenses for remote handling and diagnostic optical transmission systems, Journal of Nuclear Materials. 329–333 (2004) 1438–1441. https://doi.org/10.1016/j.jnucmat.2004.04.163.

[8] S.M. González de Vicente, E.R. Hodgson, T. Shikama, Functional materials for tokamak in-vessel systems—status and developments, Nucl. Fusion. 57 (2017) 092009. https://doi.org/10.1088/1741-4326/aa6a5d.

[9] T. Allanche, Effect of high radiation doses (MGy) on Light Emitting Diodes and optical glasses, Univ de lyon, 2021. https://tel.archives-ouvertes.fr/tel-03215958.

[10] I. Manolis, J.-L. Bézy, R. Vink, R. Meynart, The ESA radglass activity: a radiation study of non rad-hard glasses, in: Proc. of SPIE, 2016: pp. 1056214-1-1056214–9. https://doi.org/10.1117/12.2296084.

[11] I. Manolis, J.-L. Bézy, A. Costantino, R. Vink, A. Deep, M. Ahmad, E. Amorim, M.D. Miranda, R. Meynart, The ESA RADGLASS activity: a radiation study of non rad-hard glasses, in: R. Meynart, S.P. Neeck, H. Shimoda (Eds.), Proc. SPIE, Proc. SPIE, 2015: p. 96391N. https://doi.org/10.1117/12.2193913.

[12] A. Cline, C. McNiel, P. Reyes, P. Shubert, Optical Design for Thermal and Radiation Effects in Space Optical Communication Systems, in: 2019 IEEE International Conference on Space Optical Systems and Applications (ICSOS), IEEE, Portland, OR, USA, 2019: pp. 1–4. https://doi.org/10.1109/ICSOS45490.2019.8978988.

[13] R. Jedamzik, U. Petzold, SCHOTT optical glass in space, in: P. Hallibert, T.B. Hull, D.W. Kim (Eds.), Astronomical Optics: Design, Manufacture, and Test of Space and Ground Systems, SPIE, San Diego, United States, 2017: p. 16. https://doi.org/10.1117/12.2272714.

[14] S.-F. Lin, C.-H. Chen, Optical Design of Compact Space Autonomous Docking Instrument with CMOS Image Sensor and All Radiation Resistant Lens Elements, Applied Sciences. 10 (2020) 5302. https://doi.org/10.3390/app10155302.

[15] C. Muller, T. Allanche, A. Boukenter, P. Paillet, S. Girard, Y. Ouerdane, T. Lépine, Potential performance loss and compensation techniques of a lens under ionizing radiations, in: L. Mazuray, R. Wartmann, A.P. Wood (Eds.), Optical Design and Engineering VII, SPIE, Frankfurt, Germany, 2018: p. 24. https://doi.org/10.1117/12.2313245.

[16] C. Muller, T. Allanche, P. Paillet, O. Duhamel, V. Goiffon, S. Rizzolo, T. Lépine, J. Rousson, J.-P. Baudu, J.-R. Macé, H. Desjonqueres, C. Monsanglant Louvet, Y. Ouerdane, A. Boukenter, S. Girard, Investigations of the MGy dose level radiation effects on the photometric budget of a radiation-hardened CMOS-based camera, Appl. Opt. 58 (2019) 6165. https://doi.org/10.1364/AO.58.006165.

[17] C. Muller, Conception optique pour les environnements radiatifs et application à une caméra résistante à des doses élevées (MGy), CAMRAD, n.d.

[18] S. Girard, T. Allanche, P. Paillet, V. Goiffon, M. Van Uffelen, L. Mont-Casellas, C. Muller, A. Boukenter, Y. Ouerdane, W. De Cock, Growth and Decay Kinetics of Radiation-Induced Attenuation in Bulk Optical Materials, IEEE Transactions on Nuclear Science. 65 (2018) 1612–1618. https://doi.org/10.1109/TNS.2017.2778318.

[19] Ohara, Press Release : Non-Browning Optical Glass Has Released, 12AD. https://web.archive.org/web/20161020150229/https://www.ohara-inc.co.jp/en/news/images/151222_NonBrowingGlass_PressRelease_Final_Eng.pdf (accessed May 13, 2020).

[20] Non-Browning Optical Glass, Ohara-Gmbh. (2021). https://www.ohara-gmbh.com/fileadmin/user_upload/non_browning_glass.pdf (accessed February 19, 2021).

[21] CDGMGD, Optical Glass(PDF)201904new, (n.d.). http://www.cdgmgd.com/downloadFile.htm?id=12981 (accessed January 27, 2020).

[22] T.D. Henson, G.K. Torrington, Space radiation testing of radiation-resistant glasses and crystals, in: A.J. Marker III, M.J. Davis (Eds.), San Diego, CA, 2001: pp. 54–65. https://doi.org/10.1117/12.446894.

[23] S. Girard, A. Morana, A. Ladaci, T. Robin, L. Mescia, J.-J. Bonnefois, M. Boutillier, J. Mekki, A. Paveau, B. Cadier, E. Marin, Y. Ouerdane, A. Boukenter, Recent advances in radiation-hardened fiber-based technologies for space applications, J. Opt. 20 (2018) 093001. https://doi.org/10.1088/2040-8986/aad271.

[24] D. Doyle, Radiation-induced transmission degradation of borosilicate crown optical glass from four different manufacturers, Optical Engineering. 46 (2007) 043004. https://doi.org/10.1117/1.2722322.

[25] E. Hecht, A.R. Ganesan, Optics, 2012.

[26] D. Doyle, Radiation Hardeness of Optical Materiel, (2010).

[27] D.L. Griscom, M.E. Gingerich, E.J. Friebele, Model for the Dose, Dose-Rate and Temperature Dependence of Radiation-Induced Loss in Optical Fibers, (n.d.) 5.

[28] Schott Ltd, Technical note: Radiation Resistant Optical Glasses, 2007. http://www.couriertronics.com/docs/notes/General_Machine_Vision_Appnotes/TIE-42_Radiation_resistant_glasses_%281%29.pdfhttp://www.couriertronics.com/docs/notes/General_Machine_Vision_Appnot es/TIE-42_Radiation_resistant_glasses_%281%29.pdf.

[29] A. Floriduz, J.D. Devine, Modelling of proton irradiated GaN-based high-power white light-emitting diodes, Japanese Journal of Applied Physics. 57 (2018) 080304. https://doi.org/10.7567/JJAP.57.080304.

[30] J.D. Devine, A. Floriduz, Radiation hardening of LED luminaires for accelerator tunnels, in: 2016 16th European Conference on Radiation and Its Effects on Components and Systems (RADECS), IEEE, Bremen, 2016: pp. 1–6. https://doi.org/10.1109/RADECS.2016.8093210.

[31] D. Doyle, Radiation Hardeness of Optical Materials, (2010). https://www.google.com/url?sa=t&rct=j&q=&esrc=s&source=web&cd=1&ved=2ahUKEwj0v4a4rZPhAhWo1eAKHbuaBZkQFjAAegQIARAC&url=http%3A%2F%2Fsci.esa.int%2Fscience-e%2Fwww%2Fobject%2Fdoc.cfm%3Ffobjectid%3D46396&usg=AOvVaw0CHaqg7SFSM3GR6kAwf4tO (accessed March 21, 2019).

[32] S. Girard, T. Allanche, A. Boukenter, Procédé de fabrication d'un dispositif de mesure optique apte à fonctionner sous rayonnement ionisant et dispositif de mesure optique apte à fonctionner sous rayonnement ionisant, FR1908146, n.d.

[33] S. Baccaro, A. Cemmi, I. Di Sarcina, F. Menchini, Gamma Rays Effects on the Optical Properties of Cerium-Doped Glasses, International Journal of Applied Glass Science. 6 (2015) 295–301. https://doi.org/10.1111/ijag.12131.

[34] Mirion technology, nuclear camera, Hyperion, Mirion. (n.d.). https://mirion.s3.amazonaws.com/cms4_mirion/files/pdf/spec-sheets/ops-761_hyperion_datasheet_v.4.pdf?1553795714.

[35] resolv Optic, 357-000 6.5 – 65 mm f/1.8 Non-Browning Zoom Lens, (n.d.). https://www.resolveoptics.com/6-5-65mm-f1-8-non-browning-zoom-lens/.

[36] resolv Optic, Important Considerations When Designing Optical Systems for Space Projects, (n.d.). https://www.resolveoptics.com/designing-optical-systems-for-space-projects/.

[37] SCHOTT, Radiation Resistant Optical Glasses, 2007. http://www.schott.com/d/advanced_optics/0bdd65d7-4d93-4d35-927a-a22fc6044d8e/1.2/schott_tie-42_radiation_resistant_optical_glasses_us.pdf.

[38] A. Bishay, Gamma Irradiation Studies of Some Borate Glasses, Journal of the American Ceramic Society. 44 (1961) 289–296. https://doi.org/10.1111/j.1151-2916.1961.tb15380.x.

[39] N.J. Kreidl, J.R. Hensler, Formation of color centers in glasses exposed to gamma radiation, Journal of the American Ceramic Society. 38 (1955) 423–432.

[40] P.W. Levy, Overview Of Nuclear Radiation Damage Processes: Phenomenological Features Of Radiation Damage In Crystals And Glasses, in: P.W. Levy (Ed.), Proc. SPIE, 1985: pp. 2–24. https://doi.org/10.1117/12.975356.

[41] A. Bishay, Radiation induced color centers in multicomponent glasses, Journal of Non-Crystalline Solids. 3 (1970) 54–114. https://doi.org/10.1016/0022-3093(70)90106-7.